

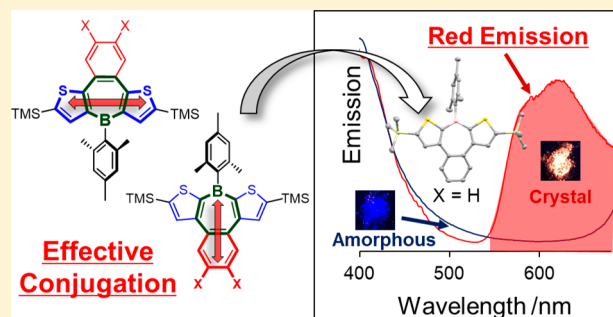
Synthesis and Properties of Benzo[*d*]dithieno[*b,f*]borepins

Yohei Adachi and Joji Ohshita*[✉]

Department of Applied Chemistry, Graduate School of Engineering, Hiroshima University, Higashi-Hiroshima 739-8527, Japan

S Supporting Information

ABSTRACT: Borepin is a seven-membered unsaturated ring system containing a tricoordinate boron. Although many borepin compounds annulated with aromatic systems have been reported to date, only one [*b,d,f*]-annulated tetracyclic borepins has been synthesized. In the present study, we synthesized benzo[*d*]-dithieno[*b,f*]borepins as a new class of building blocks for functional materials motivated by the following structural features: (1) the high chemical stability of dithieno[*b,f*]borepin species; (2) the highly conjugated tetracyclic system with a borepin ring; and (3) electronic structures that are easily tuned by the introduction of functional groups on the annulated benzene ring. The prepared borepins were stable in air both in solution and as solids, and the electronic states could be finely tuned by changing the substituents on the benzene ring. Interestingly, DFT calculations revealed that the LUMO and LUMO+1 energy levels were strongly affected by the benzo[*d*]-annulation, depending on the boron-bridged positions on the fused thiophene rings. NICS and HOMA methods proved that the aromaticity of the borepin ring in the benzo[*d*]dithieno[*b,f*]borepin system is relatively small. We also report an unexpected red emission observed for the first time in borepin compounds for benzo[*d*]dithieno[*b,f*]borepin in the solid state.



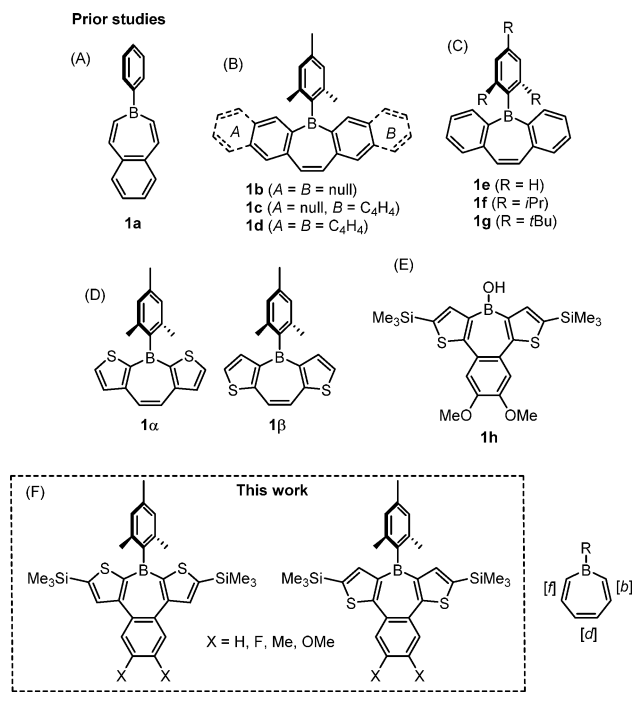
INTRODUCTION

Borepin, which is an unsaturated seven-membered ring system with tricoordinate boron, has been investigated because it has interesting aromaticity. Unlike other heteropins, such as phosphopin and silepin, the borepin system in its neutral state has an unoccupied p-orbital on boron that associates with π and π^* orbitals of the heptatriene moiety, leading to an isoelectronic state with a tropylium cation. This fulfills the requirements for Hückel aromaticity of 6π electrons, resulting in a planar structure. Much effort has been devoted to theoretical¹ and experimental approaches to examining the nature of borepin aromaticity.^{2–7} For example, Leusink and co-workers clearly demonstrated the aromaticity of 3-phenylbenzo[*d*]borepin **1a** (Chart 1A) by ¹H NMR and absorption spectroscopy in 1967.² The aromaticity of borepin improves the chemical stability. Tricoordinate boron species are usually unstable and rarely able to be handled in air, unless the boron center is kinetically stabilized by extremely bulky protecting groups, such as 2,4,6-tri-isopropylphenyl (tripyl),^{8,9} 2,4,6-tri-*t*-butylphenyl (Mes*),¹⁰ and 2,4,6-tris(trifluoromethyl)phenyl (FMe₃).¹⁰ Despite compound **1a** not having a sterically large group on the boron center, it was stable in air for several days in the solid state, strongly implying that the aromaticity stabilized the tricoordinate boron center.²

Currently, π -electron systems bridged by nonconventional heteroatoms, such as boron, silicon, germanium, and phosphorus, have received much attention as a new strategy to develop building units for π -conjugated functional materials.¹¹ Orbital interactions and/or electronic and structural perturbations by heteroatoms make it possible to control

the properties of the systems, leading to desired functionalities.^{12–14} In this regard, borepin has been studied as a bridging unit of π -electron systems. In 2009, the synthesis and optical properties of benzo- and naphtho-annulated borepins at the [*b*] and [*f*] C=C bonds were reported by Piers et al. (**1b–d** in Chart 1B).¹⁵ Annulation effectively extends the conjugation while retaining the planar structure. The benzo-fused compounds **1b** and **1c** emit in the blue spectrum with good quantum yields (**1b**, 70%, and **1c**, 39%, in CH₂Cl₂), suggesting potential applications as luminescent and sensor materials. Tovar and co-workers prepared dibenzo[*b,f*]borepins protected with a phenyl (**1e**), triptyl (**1f**), or Mes* (**1g**) group at the tricoordinate boron (Chart 1C).¹⁶ In contrast to the high chemical stability of **1a**, **1e** is unstable in air and must be handled in a glovebox. Borepin **1f** is also unstable under ambient conditions, despite the bulky triptyl group, and only **1g** with an extremely bulky Mes* protecting group is stable of these three borepins. These results indicate that annulation with benzene rings at the [*b*] and [*f*] positions of the borepin ring may not effectively stabilize the borepin system. In 2014, Tovar's group also reported the synthesis of thiophene-annulated borepins (**1a** and **1b** in Chart 1D).¹⁷ Surprisingly, although these compounds possess only a mesityl (2,4,6-trimethylphenyl) group, which is less bulky than the triptyl and Mes* groups, they are reasonably stable for several months under ambient conditions, indicating the large stabilizing effect of the thiophene annulation. In addition to these reports, many

Received: November 23, 2017

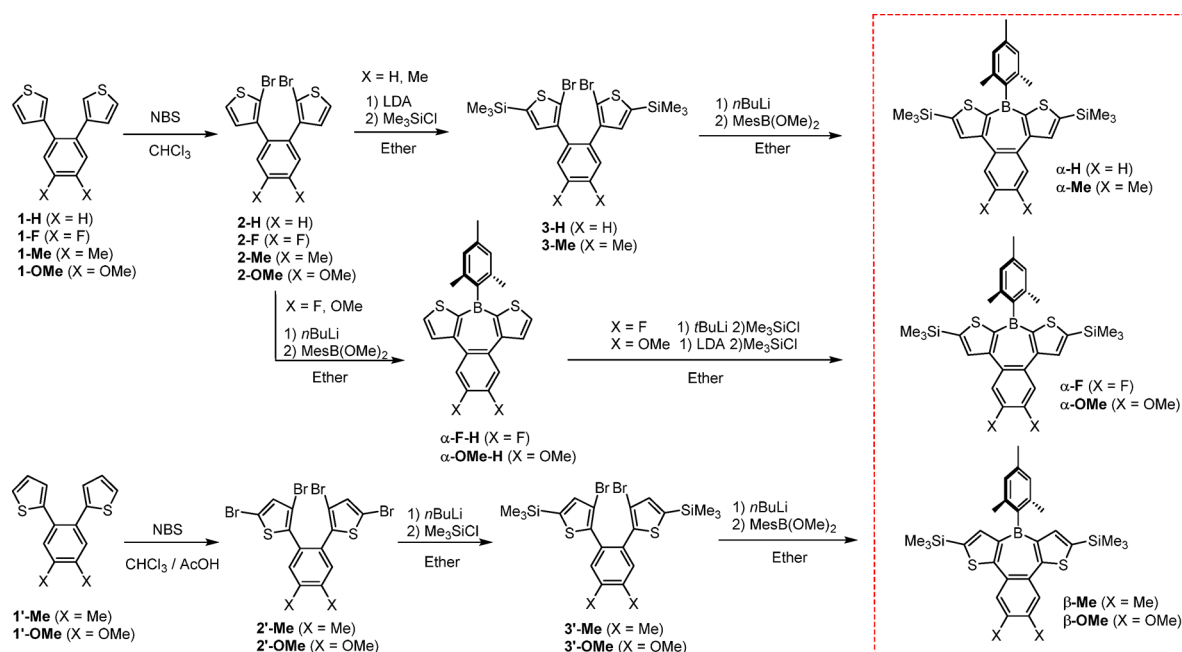
Chart 1. Reported Structures of Borepins Fused with Aromatic Systems


other borepin compounds annulated with aromatic systems, including benzene,^{2,3,15,16,18a–d,19,21} thiophene,^{5,6,17,18d,e,21} benzothiophene,^{18f} pyrrole,⁷ naphthalene,^{15,18d,20} acenaphthene,²⁰ and acenaphthylene²⁰ have been reported. However, in most reports, the annulated borepins were $[bf]$ -annulated tricyclic or $[d]$ -annulated bicyclic systems. To our knowledge, no $[b,d,f]$ -annulated tetracyclic borepins have been reported, except for borinic acid compound **1h** (Chart 1E).²¹ In borepin **1h**, electron donation from the adjacent oxygen diminishes the vacancy of the boron p-orbital, thereby suppressing the

aromaticity. In addition, the detailed properties of **1h**, including the crystal structure and electrochemical properties have not been reported. Therefore, the fundamental nature of $[b,d,f]$ -annulated tetracyclic borepins has not been elucidated. In this work, we introduced benzo-annulation at the $[d]$ position of dithieno $[bf]$ borepin with a mesityl group on the boron as a protecting group. We investigated the effects of benzo $[d]$ -annulation on the stability, electronic states, aromaticity, and photophysical properties of the dithieno $[bf]$ borepins. We expected that introducing functional groups on the annulated benzene ring at the borepin $[d]$ position would be an effective way to finely tune the electronic state of the borepin system. It was also anticipated that extending the π -conjugated system at the $[d]$ position would enhance the π - π intermolecular interaction in the condensed phase, which may result in optoelectronic properties such as semiconducting behaviors in the solid state. Benzo $[d]$ dithieno $[bf]$ borepins with a mesityl group were prepared (Chart 1F), which showed high chemical stability for several months in the solid state and for several weeks in solution. The optical and electrochemical properties were examined in detail and are discussed, along with computer simulation results. The crystal structures were solved by single-crystal X-ray diffraction analysis. We also report an unexpected red emission in the crystal state.

RESULTS AND DISCUSSION

Synthesis. The synthetic route toward tetracyclic benzo $[d]$ dithieno $[bf]$ borepins is shown in Scheme 1 and included dilithiation of the corresponding bis(bromothieryl)benzenes, followed by quenching with $\text{MesB}(\text{OMe})_2$ in ether in moderate yields. The reaction solvent seems to be very important because Lee et al. reported that a similar synthetic protocol in THF was unsuccessful in the synthesis of the β -OMe compound.²¹ Various groups (H, F, Me, and OMe) were introduced at the 4,5-positions on the annulated benzene ring. Trimethylsilyl groups were introduced to the external α -positions of the thiophene rings in the expectation that the chemical stability

Scheme 1. Synthetic Route toward Benzo $[d]$ dithieno $[bf]$ borepins


would be improved by kinetic stabilization of the borepin ring and capping of the reactive thiophene α -positions. We also attempted the synthesis of β -bridged benzo[*d*]dithieno[*b,f*]-borepins possessing H or F atoms on the annulated benzene ring. However, the attempted tetra-bromination of 1,2-bis(2-thienyl)benzene with 4 equiv of *N*-bromosuccinimide (NBS) provided a complex mixture, and the similar tetra-bromination of 1,2-di(2-thienyl)-4,5-difluorobenzene gave the α -dibrominated compound as the sole isolable product. The dilithiations of 2-F and 2-OMe with lithium diisopropylamide (LDA) were unsuccessful, providing complex mixtures, and the corresponding trimethylsilyl-substituted bis(bromothiophenyl)benzene precursors could not be prepared. Therefore, unlike compounds α -H, α -Me, β -Me, and β -OMe, trimethylsilyl groups were introduced onto compounds α -F and α -OMe after forming the borepin ring. Indeed, compound α -F was prepared via dilithiation of α -F-H with *t*BuLi followed by silylation. Compound α -OMe was synthesized via lithiation with LDA, because α -OMe-H was not able to be completely lithiated by *t*BuLi at low temperature. All the prepared benzo[*d*]borepin compounds (α -H, α -F, α -Me, α -OMe, β -Me, and β -OMe) were identified by NMR (Figure S1–S55) and high-resolution mass spectrometry. The compounds were stable under ambient atmospheric conditions in the solid state for at least 3 months, and no decomposition was observed in the ^1H NMR spectra. This high chemical stability is likely to be derived from the dithieno[*b,f*]- and benzo[*d*]-annulations.

To investigate the stability in solution, we monitored the ^1H NMR spectral changes in CDCl_3 . The NMR sample sealed by a Teflon tape with air was kept at room temperature under ambient light. As shown in Figures 1 and S56–S71, the α -bridged compounds are clearly more stable than the β -bridged compounds. In the spectra of β -bridged compounds, the proton signals from the mesityl groups (H_c in Figure 1) were gradually decreased, and many unidentified peaks appeared after 1 month. From the integration ratios, approximately 70% of β -Me and 60% of β -OMe were decomposed after 1 month. In contrast, in the spectra of α -bridged compounds, the integrations of H_c protons of α -Me and α -OMe remained at about 90%, and no dramatic changes were observed even after 1 month under ambient conditions. These results indicated that α -bridged borepins possessed quite high chemical stability, making their application in the synthesis of functional materials feasible. Compound α -F showed relatively low stability compared with the other α -bridged borepins, and the stability was lower than that of α -F-H (Figures S58–S60), although we had expected that the bulky trimethylsilyl group may kinetically stabilize the borepin ring.

Crystal Structures. Fortunately, we obtained crystals of the benzo[*d*]dithieno[*b,f*]borepins suitable for single-crystal X-ray diffraction analysis from appropriate solvents, except for α -OMe. Numbering the carbons in the present borepin structures is shown in Chart 2. Figure 2 shows the crystal structures of α -H, α -Me, and β -Me as typical examples. Those of the other borepins are available in the Supporting Information (Figures S72 and S73). Selected bond lengths and dihedral angles are summarized in Table 1. The endocyclic dihedral angles ranged from 10.3 to 20.6° for the α -bridged compounds, indicating a lower degree of planarity of the borepin rings, relative to the β -bridged compounds that had dihedral angles of 3.6–9.5°. The benzene and thiophene rings were over and below the borepin ring plane (Figure 2). The lower planarity of the α -borepins compared with the β -borepins was likely due to steric repulsion

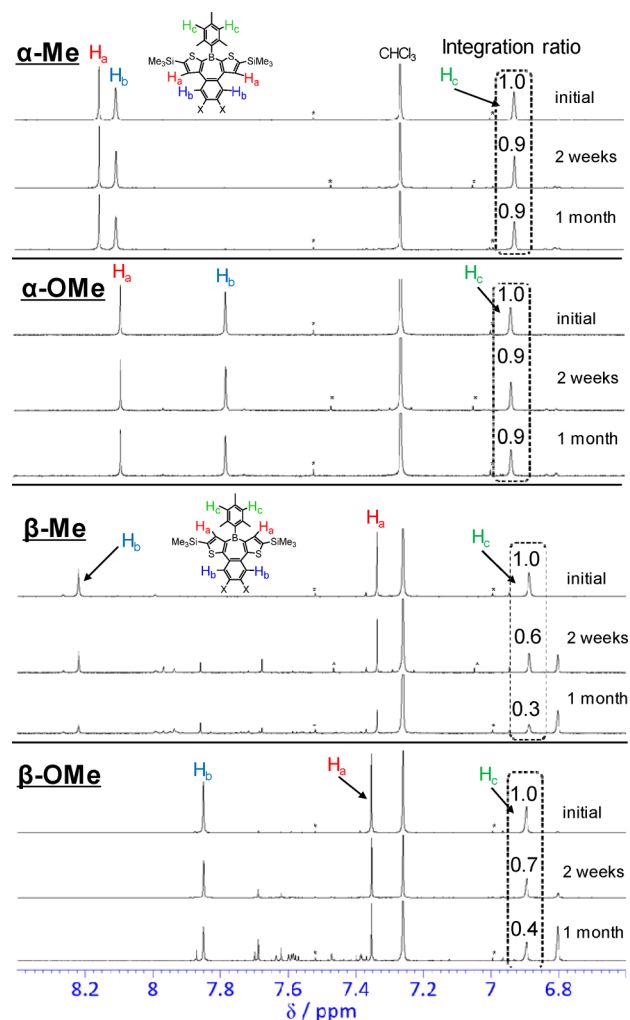
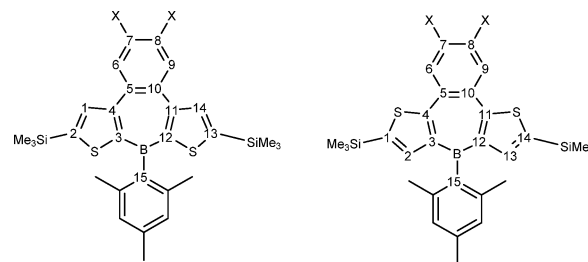


Figure 1. Aromatic regions of the ^1H NMR spectra of α -Me, α -OMe, β -Me, and β -OMe; initial, after 2 weeks, and after 1 month in CDCl_3 . The integration ratio is given relative to the initial signal. The residual CHCl_3 peak was used as the integration standard.

Chart 2. Structural Representation of the Present Borepins



between the phenylene and thiophene C–H bonds. As shown in Figures 2 and S73, β -Me and β -OMe have π -stacked packing crystal structures with π – π distances of 3.621 Å for β -Me and 3.686 Å for β -OMe. As no clear π – π interaction was observed in the crystal structure of 1β ,¹⁷ the extended π -conjugation by the benzo[*d*]-annulation seemed to enhance π – π interaction in this system. In contrast, the α -bridged borepins (α -H, α -F, and α -Me) did not exhibit π -stacking in the crystal structures. All endocyclic B–C3 and B–C12 bonds of the synthesized borepins were shorter than the exocyclic B–C15 (Mes) bonds (Table 1), indicating delocalization of the π -electrons

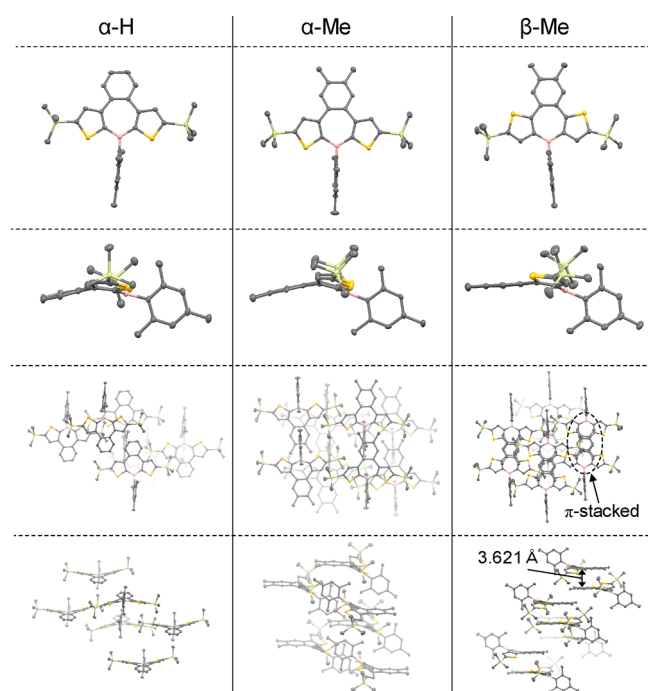
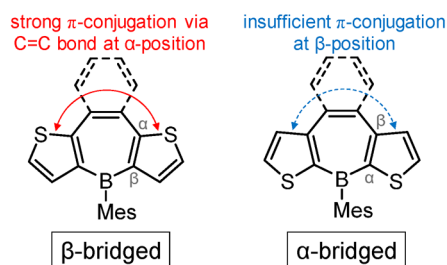


Figure 2. Crystal structures and packing diagrams of α -H (left), α -Me (middle), and β -Me (right) obtained at 123 K. Thermal ellipsoids are at the 50% probability level. Hydrogen atoms are omitted for clarity.

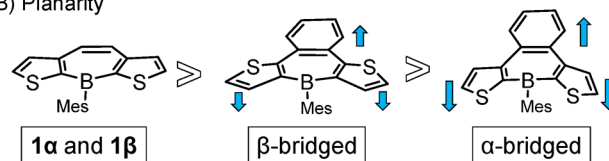
in the borepin rings. However, these endocyclic B–C bonds are slightly longer than those of **1 α** (1.522(2) and 1.521(2) Å) and **1 β** (1.533(2) and 1.538(2) Å).¹⁷ This difference suggests the tetracyclic borepins have relatively little aromaticity compared with **1 α** and **1 β** , likely because of the high aromaticity of the annulated benzene rings, which suppresses the aromaticity of the borepin rings. Similar electronic confinement has also been reported for phosphepin derivatives.²² Phosphepins annulated with a nonaromatic ring at the [d] position showed more extended conjugation than phosphepins annulated with an aromatic ring at the same position. As **1 β** was reported to have a highly planar structure, the relatively low planarity of **β -Me** and **β -OMe**, which have no steric repulsion between the phenylene and thiophene C–H bonds, can be explained by the low aromaticity of the borepin ring derived from the annulation of a highly aromatic benzene ring. Similar deviation of planarity induced by benzo[d]-annulation was theoretically predicted in dibenzo[b,f]borepin species.¹⁴

Optical Properties. Three important factors affect the borepin electronic states (Figure 3). First, β -bridged borepins have effective π -conjugation between the two thiophene rings through the α,α' -ethynylene linkage, whereas α -bridged borepins with a β,β' -ethynylene linkage have less effective conjugation between the thiophene rings (Figure 3A). This

A) Conjugation (α vs β)



B) Planarity



C) π -Extension (benzo[d]-annulation)

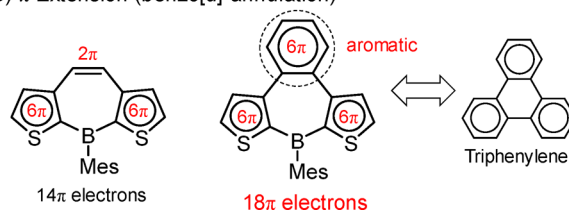


Figure 3. Considerable competing factors affecting the photophysical properties of the present borepins.

difference essentially gives rise to smaller HOMO–LUMO gaps for the β -bridged compounds. Indeed, **1 β** has a longer wavelength at the absorption onset (390 nm) than that of **1 α** (378 nm) in CHCl_3 solution.¹⁷ Second, the planarity of the compounds has an effect (Figure 3B). As we found in the single-crystal structures of the borepins, the planarity changes depending on the bridging positions; for example, **β -Me** exhibited higher planarity than **α -Me**. Finally, benzo-[d] annulation usually extends the conjugation to minimize the HOMO–LUMO energy gap (Figure 3C). Benzo-[d] annulated borepin has similar Clar structure²³ to triphenylene, suggesting that the borepin ring in benzo-[d] annulated system has weak aromaticity similar to the center ring in triphenylene²⁴ (Figure 3C), which also exerts influence on the electronic states of the whole systems. Similar effects of Clar structure on fused borepins have been recently reported.^{18f} Furthermore, the donor–acceptor (D–A) interaction through the benzo[d]-borepin core may affect the electronic states.

The absorption spectra of the borepins in THF are shown in Figure 4. All spectra possessed multiple bands with shoulder peaks in the region of 250–430 nm. For the α -bridged compounds, the absorption edge of α -F was at almost the same energy as that of α -H, whereas α -Me and α -OMe had red-

Table 1. Selected Bond Lengths and Dihedral Angles Obtained from X-ray Analysis

	bond length (Å)					dihedral angle (deg)	
	B–C3, B–C12	C3–C4, C11–C12	C4–C5, C10–C11	C5–C10	B–C15	B–C3=C4–C5, B–C12=C11–C10	
α -H	1.514(3), 1.531(2)	1.407(2), 1.410(2)	1.478(2), 1.475(3)	1.426(3)	1.591(2)	10.9, 13.4	
α -F	1.532(2), 1.524(2)	1.399(2), 1.397(2)	1.475(2), 1.478(2)	1.420(2)	1.579(2)	10.3, 20.6	
α -Me	1.525(3), 1.530(3)	1.399(2), 1.399(2)	1.472(3), 1.471(3)	1.428(2)	1.586(3)	16.3, 15.4	
β -Me	1.533(3), 1.543(2)	1.400(2), 1.400(3)	1.465(2), 1.460(3)	1.419(3)	1.589(3)	9.5, 4.7	
β -OMe	1.534(3), 1.532(3)	1.398(2), 1.400(2)	1.466(2), 1.466(3)	1.417(3)	1.592(2)	4.7, 3.6	

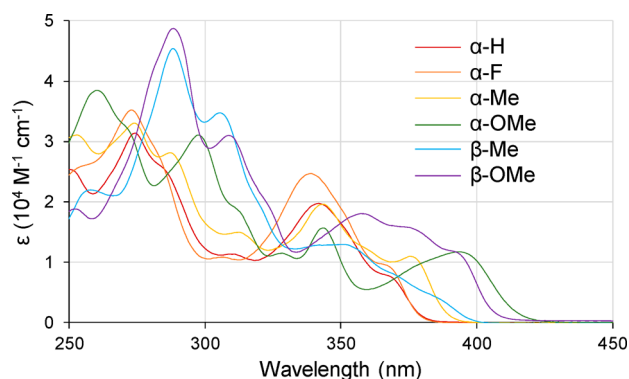


Figure 4. Absorption spectra of benzo[*d*]-annulated borepins in THF.

shifted edges compared with those of α -H and α -F. Borepins α -OMe and β -OMe, with electron-donating methoxy groups, showed relatively red-shifted absorptions compared with those of other borepins. The onset wavelengths of the absorptions were shifted to longer wavelengths in the order of α -F \leq α -H $<$ α -Me $<$ β -Me $<$ β -OMe $<$ α -OMe. As the spectra varied depending on the substituents on the benzene ring, it appears that the substituents on the benzene ring can tune the electronic structure of the whole borepin system. We predicted that β -bridged borepins would show more red-shifted absorptions compared with α -bridged compounds because of the electronic/structural features (Figure 3A,B). However, the estimated HOMO–LUMO energy gaps (E_g^{opt}) for the α -Me and β -Me pair, as well as for α -OMe and β -OMe, were almost the same. This indicated that the effect of the benzo[*d*] annulation on the energy levels strongly depended on the bridging position of the thiophene rings. This is discussed in detail later in the section on density functional theory (DFT) calculations (*vide infra*).

The fluorescence spectra of the borepins in THF are shown in Figure 5. Similar to the absorption spectra, the fluorescence

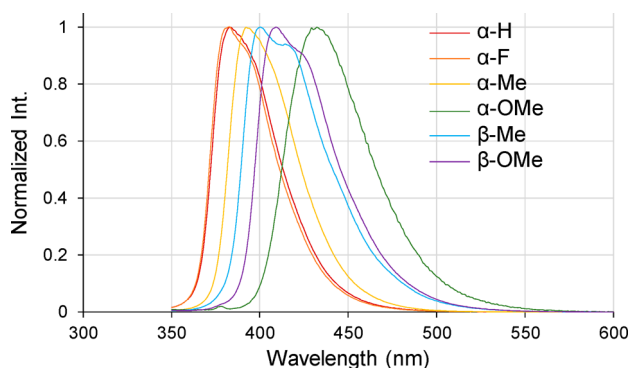


Figure 5. Fluorescence spectra of benzo[*d*]-annulated borepins in THF.

spectra of α -H and α -F were similar, but the spectra for α -Me and α -OMe showed bands in a lower energy region. The maximum wavelengths of fluorescence were shifted to longer wavelengths in the order of α -H = α -F $<$ α -Me $<$ β -Me $<$ β -OMe $<$ α -OMe, which is almost consistent with the order of the absorption edge. In the spectra of β -Me and β -OMe, vibronic bands were clearly observed, likely because of the higher structural rigidity of the β -bridged borepins compared with the α -bridged compounds. This consideration is consistent with the highly planar structure of the β -bridged borepins

obtained from X-ray diffraction analysis. The fluorescence quantum yields were low, at 2% for β -Me and too weak to determine ($<2\%$) for the other borepins (Table 2). Similar

Table 2. Optical and Electrochemical Properties of Benzo[*d*]-Annulated Borepins

sample	$\lambda_{\text{onset}}^{\text{abs}}$ (nm) ^a	E_g^{opt} (eV) ^b	$\lambda_{\text{max}}^{\text{em}}$ (nm)	Φ (%)	τ (ns) ^d	E_{red} (V)	E_{ox} (V) ^f
α -H	381	3.25	383	<i>g</i>	0.25	−2.08	0.90
α -F	379	3.27	383	<i>g</i>	0.21	−2.03	<i>h</i>
α -Me	390	3.18	392	<i>g</i>	0.30	−2.13	0.94
α -OMe	415	2.99	432	<i>g</i>	0.22	−2.14	0.73
β -Me	399	3.11	400	2	1.01	−2.24	0.98
β -OMe	407	3.05	409	<i>g</i>	0.46	−2.26	0.79

^aAbsorption onset in 0.02 mM THF solution. ^b E_g^{opt} (eV) = 1240/ $\lambda_{\text{onset}}^{\text{abs}}$ (nm) ^cIn 0.02 mM THF solution, excited at 340 nm. ^dEmission lifetime, excited at 318 nm. ^eReductive potential (vs Fc/Fc⁺) obtained from the onset of cathodic wave. ^fOxidative potential (vs Fc/Fc⁺) obtained from the onset of anodic wave. ^gToo weak to determine. ^hNot detected.

barely emissive properties in solution have been reported for **1 α** (Φ = 5%) and **1 β** (Φ = 6%).¹⁷ The fluorescence lifetimes were quite short, ranging from 0.21 to 1.01 ns. As compounds α -OMe and β -OMe possessed electron-donating methoxy groups with the electron-deficient borepin system, a D–A interaction may be induced. We measured the fluorescence spectra of α -OMe and β -OMe in toluene and DMF in addition to THF (Figure S74). The spectra of α -OMe were shifted to longer wavelengths as the solvent polarity increased, which was likely derived from the intramolecular charge transfer (ICT) character of the photoexcited state, indicating an intramolecular D–A interaction. In contrast, the spectra of β -OMe were broadened in polar solvents; however, the fluorescence bands were observed at similar wavelengths regardless of the solvent polarity. This indicates that the electronic interaction between the annulated benzene moiety and the dithieno[*b,f*]borepin system is very different depending on the bridging position. Even though the benzo[*d*]-annulated borepins have potentially more extended conjugation than **1 α** and **1 β** from the benzo[*d*] annulation (Figure 3C), the red-shifts of absorption edge and fluorescence wavelengths were slight, which was probably due to competition between the lower planarity and higher π -extension, which balance each other out. The trimethylsilyl groups might also contribute to the slight red-shift. Indeed, the absorption edges of α -F-H (372 nm) and α -OMe-H (406 nm) in THF were slightly blue-shifted from those of the corresponding silylated borepins α -F and α -OMe.

DFT Calculations and Evaluations of Aromaticity. To further investigate the electronic structures of the tetracyclic borepins, we carried out DFT calculations at the B3LYP/6-31G(d) level of theory on the Gaussian 09 program. We also performed calculations for the model compounds **1 α -Si** and **1 β -Si** without benzo[*d*] annulation for comparison (Figure 6). The calculated HOMO and LUMO energy levels and the dihedral angles of the optimized structures are summarized in Table 3. Similar to the crystal structures, the optimized structures possessed nonplanar benzo[*d*]-annulated borepin systems, whereas **1 α -Si** and **1 β -Si** were completely planar (Table 3). α -Me and α -OMe had higher HOMO energy levels, while α -F had a lower LUMO level, than those of α -H. These energy shifts clearly reflected the electronic properties of the substituents, that is, electron-donating methyl and methoxy

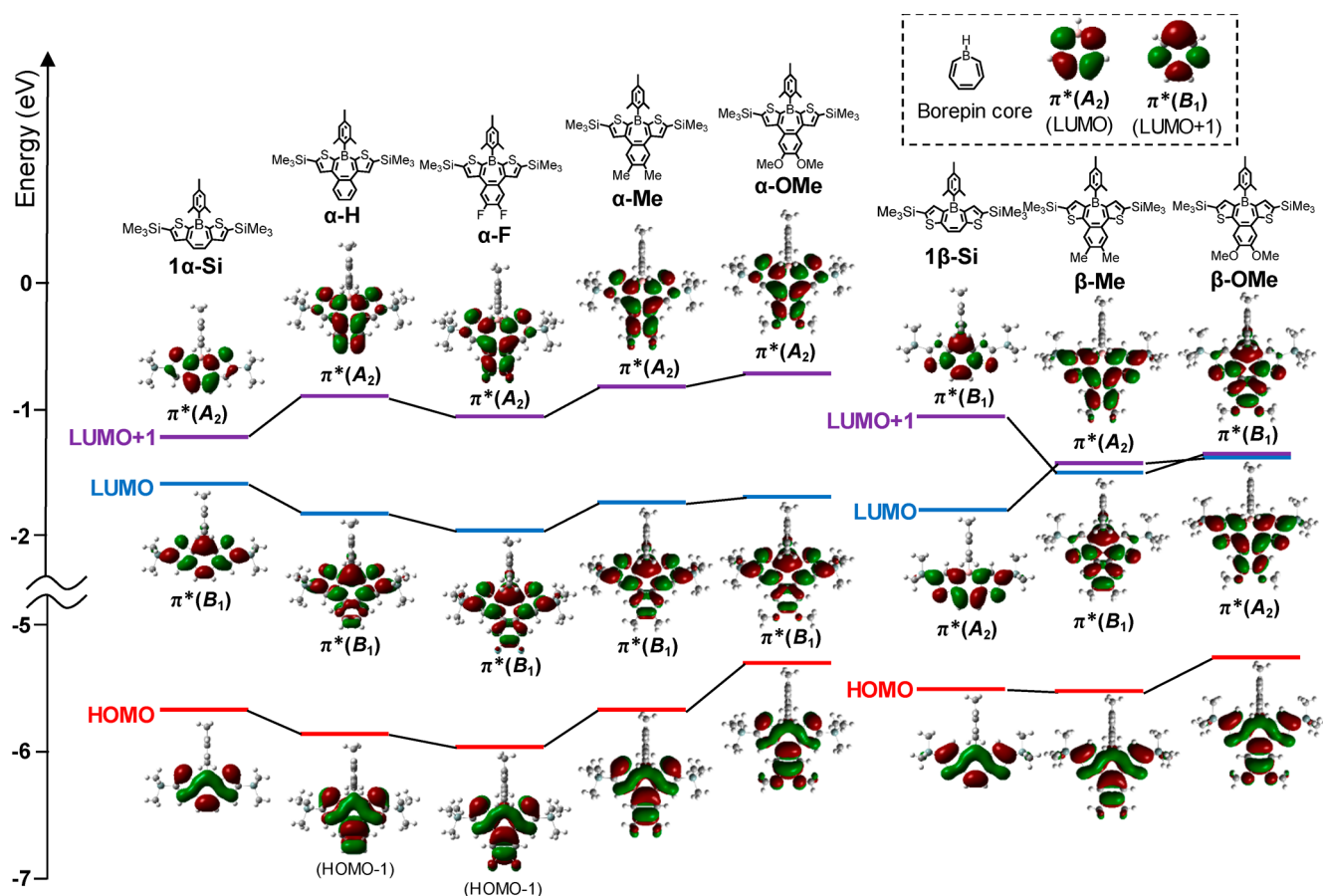


Figure 6. Frontier orbitals of the borepin core and dithieno[*b,f*]borepins calculated from DFT at B3LYP/6-31G(d) level of theory. HOMO–1 is shown for α -H and α -F because the HOMOs are localized on the mesityl group.

Table 3. Calculated Parameters of Dithieno[*b,f*]borepins

	dihedral angle (deg) ^a	HOMO (eV) ^b	LUMO (eV) ^b	LUMO+1 (eV) ^b	$\Delta E_{(L-L+1)}$ (eV) ^c	E_g^{theo} (eV) ^d
1α-Si	0.0	−5.68	−1.60	−1.24	0.36	4.08
α-H	15.9	−5.86 ^e	−1.81	−0.94	0.87	4.05
α-F	15.3	−5.96 ^e	−1.96	−1.10	0.87	4.00
α-Me	15.4	−5.69	−1.74	−0.86	0.87	3.95
α-OMe	15.1	−5.32	−1.68	−0.76	0.92	3.63
1β-Si	0.0	−5.53	−1.81	−1.09	0.72	3.72
β-Me	10.5	−5.54	−1.49	−1.46	0.04	4.05
β-OMe	10.4	−5.28	−1.40	−1.39	0.01	3.88

^aBetween B–C3=C4–C5 as shown in Table 1 and Chart 2. ^bDFT calculated at B3LYP/6-31G(d) level. ^cEnergy gap between LUMO and LUMO +1. ^dEnergy gap between HOMO and LUMO. HOMO–1 is used for α -H and α -F because the HOMOs are localized on the mesityl group. ^eHOMO–1 because the HOMO is localized on the mesityl group.

substituents and electron-withdrawing fluorine atoms. The calculated HOMO–LUMO energy gap (E_g^{theo}) of **1 β -Si** was smaller than that of **1 α -Si**, which derived from the conjugated thiophene system of **1 β -Si** (Figure 3A). In contrast, despite the effective conjugation and higher planarity of the β -bridged compounds, the E_g^{theo} values for α -Me and β -Me and for α -OMe and β -OMe, were almost the same. These calculated results are consistent with the experimentally estimated energy gaps (E_g^{opt}), as discussed above. The calculated frontier orbitals are shown in Figure 6. The HOMOs of the dithieno[*b,f*]borepins were similar regardless of the bridged position and benzo[*d*]annulation. In contrast, the LUMOs could be classified into two orbital symmetries based on $\pi^*(A_2)$ and $\pi^*(B_1)$ orbitals of the borepin core. The LUMO of the α -

bridged borepins and β -Me had $\pi^*(B_1)$ symmetry, whereas $\pi^*(A_2)$ symmetry was observed in the LUMO of **1 β -Si** and β -OMe. Meanwhile, the LUMO+1s of the borepins had opposite symmetry ($\pi^*(A_2)$ or $\pi^*(B_1)$) to the LUMOs. This indicated that the LUMO and LUMO+1 of the dithieno[*b,f*]borepins were composed of the $\pi^*(A_2)$ or $\pi^*(B_1)$ symmetry of the borepin core and that these energy levels were strongly influenced by the bridged position (α - or β -) and benzo[*d*]annulation. As compared with the benzo[*d*]annulated or nonannulated compounds, the LUMO energy levels of the α -bridged borepins were clearly lowered by benzo[*d*]annulation, whereas the LUMO+1 energy levels were raised. In contrast, the LUMO energy levels of the β -bridged compounds were elevated by benzo[*d*]annulation, and LUMO+1 energy levels

were lowered. These LUMO and LUMO+1 energy shifts are clearly shown by the energy differences between the LUMO and LUMO+1 ($\Delta E_{(L-L+1)}$) in Table 3. For example, as a result of these energy shifts, β -Me and β -OMe had $\Delta E_{(L-L+1)}$ values of only 0.04 and 0.01, respectively. When we compared these energy shifts with the orbital symmetry, we found that benzo[*d*]-annulation effectively lowered the energy level of the $\pi^*(B_1)$ symmetry orbital, whereas annulation raised the $\pi^*(A_2)$ symmetry orbital energy level. To elucidate the effects of benzo[*d*]-annulation on the LUMO and LUMO+1 energy levels, we performed DFT calculations on the simple benzo[*d*]borepin compound without thiophene annulations (Figure 7). As predicted, in the benzo[*d*]borepin system, the

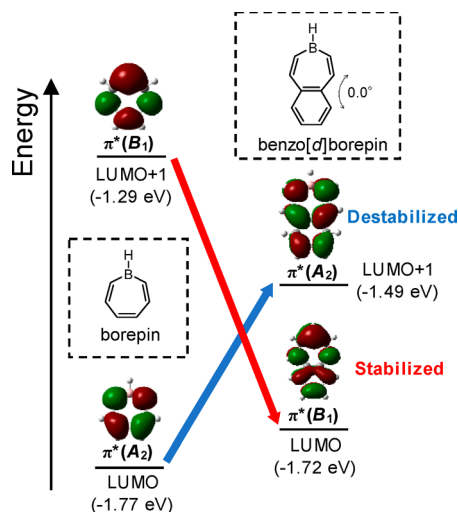


Figure 7. Energy diagrams of 3H-benzo[*d*]borepin calculated from the DFT at B3LYP/6-31G(d) level of theory.

$\pi^*(B_1)$ symmetry orbital (LUMO) was stabilized, and the $\pi^*(A_2)$ symmetry orbital (LUMO+1) was destabilized from the original borepin core π^* orbitals, which was consistent with the results of calculations for the present dithieno[*b,f*]borepin systems. As **1 α -Si** and **1 β -Si** possess $\pi^*(B_1)$ and $\pi^*(A_2)$ -based LUMOs, respectively, the benzo[*d*]-annulation provided effective stabilization of the $\pi^*(B_1)$ -based LUMO for the α -bridged borepins, whereas annulation destabilized the $\pi^*(A_2)$ -based LUMO for the β -bridged borepins. As a result of competition between the effects of the bridged position, the planarity, and the orbital symmetry of the LUMO and LUMO +1, the α -bridged borepins showed similar HOMO–LUMO

energy gaps to the β -bridged compounds. It was also noted that the $\pi^*(B_1)$ orbital clearly involved the vacant tricoordinate boron p-orbital, while the $\pi^*(A_2)$ did not. As the boron p-orbital contributed less to the HOMO than the $\pi^*(B_1)$ orbital, the $\pi^*(B_1)$ orbital played a role in the D–A interaction, and the HOMO– $\pi^*(B_1)$ transition seemed to be responsible for the ICT state of the benzoborepins. This agreed with the fact that α -OMe with $\pi^*(B_1)$ as the LUMO showed a solvatochromic PL spectral feature, in contrast to β -OMe. Compound β -OMe had nearly degenerate $\pi^*(B_1)$ and $\pi^*(A_2)$ orbitals and did not show solvatochromic behavior.

Next, we carried out nucleus-independent chemical shift (NICS) calculations to evaluate the aromaticity of the borepin ring in the tetracyclic borepin systems. The NICS calculations were performed at B3LYP/6-31+G(d,p) level of theory. First, we computed NICS based on the optimized structures from the DFT calculations (NICS(± 1)^{theo} and NICS(0)^{theo} in Tables 4 and S1, respectively). The NICS(1)^{theo} values of **1 α -Si** and **1 β -Si** were negative enough to presume that the borepin ring possess certain aromaticity. However, the NICS(± 1)^{theo} values of the tetracyclic borepins were obviously more positive than those of **1 α -Si** and **1 β -Si**. We then performed NICS calculations based on the crystal structures obtained from the X-ray diffraction studies (NICS(± 1)^{exp} and NICS(0)^{exp} in Tables 4 and S1, respectively). The calculated NICS(± 1)^{exp} values were very similar to the corresponding NICS(± 1)^{theo}. The NICS(± 1) values depended on the side of the borepin plane the ghost atom was placed on (NICS(+1) and NICS(–1)) (Figure 8). This is due to the nonplanarity of

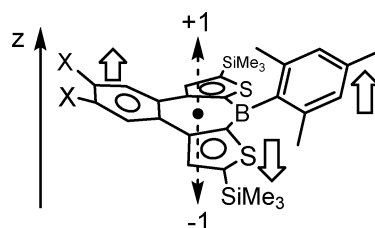


Figure 8. Schematic representation of NICS(± 1).

the tetracyclic borepin rings. However, the differences were small and nearly negligible. All the NICS values were only slightly negative, at most –3.80 ppm for NICS(–1)^{theo} of β -OMe, indicating their weak aromaticity. To confirm this lack of aromaticity, we estimated the harmonic oscillator model of aromaticity (HOMA) values using the bond lengths in the

Table 4. Calculated Parameters of Dithieno[*b,f*]borepins

	NICS(+1) ^{theo} (δ , ppm) ^{a,c}	NICS(–1) ^{theo} (δ , ppm) ^{a,d}	NICS(+1) ^{exp} (δ , ppm) ^{b,c}	NICS(–1) ^{exp} (δ , ppm) ^{b,d}	HOMA ^{theo} ^a	HOMA ^{exp} ^b
1α-Si	–4.89	<i>e</i>			0.59	(0.63) ^f
α -H	–1.69	–2.72	–2.40	–2.53	0.45	0.50
α -F	–2.19	–3.23	–1.66	–2.28	0.45	0.48
α -Me	–2.41	–3.30	–2.11	–2.66	0.46	0.50
α -OMe	–2.65	–3.59			0.48	
1β-Si	–4.51	<i>e</i>			0.54	(0.57) ^f
β -Me	–2.62	–3.38	–2.34	–3.37	0.44	0.47
β -OMe	–2.91	–3.80	–3.17	–3.15	0.46	0.49

^aBased on optimized structures from DFT calculations with respect to the borepin ring. ^bBased on crystal structures. ^cGhost atom located at 1 Å from the borepin ring center at the same direction of the mesityl group on boron. DFT calculated at B3LYP/6-31+G(d,p) level. ^dGhost atom located at 1 Å from the borepin ring center at the opposite direction of the mesityl group on boron. DFT calculated at B3LYP/6-31+G(d,p) level. ^eThe same with NICS(+1) because of the planar structure. ^fEstimated based on the X-ray data of **1 α** and **1 β** that possess no trimethylsilyl groups.¹⁷

borepin ring. The “optimal” bond length (R_{opt}) in a fully aromatic system can be estimated from eq 1 using the single (R_s) and double (R_d) bond lengths. The concept of the HOMA method is based on the difference between R_{opt} and the corresponding bond lengths in real compounds or calculated structures (R_i), as shown in eqs 1–3:

$$R_{\text{opt}} = (R_s + \omega R_d) / (1 + \omega) \quad (1)$$

$$\alpha = 2[(R_{\text{opt}} - R_s)^2 + (R_{\text{opt}} - R_d)^2]^{-1} \quad (2)$$

$$\text{HOMA} = 1 - \frac{1}{N} \sum_i \alpha (R_{\text{opt}} - R_i)^2 \quad (3)$$

where ω is taken as 2, N is the number of bonds in the cyclic system, and α is a constant for each bond type.²⁵ In general, HOMA values over 0.5 indicate aromatic, values between 0 and 0.5 indicate nonaromatic systems, and negative values indicate antiaromatic systems. First, we calculated the HOMA values of the parent rings. On the basis of the optimized structures at B3LYP/6-31G(d) level of theory, the HOMA values of 1H-borepin, thiophene, and benzene were obtained as 0.65, 0.88, and 0.99, respectively, indicating the relatively weak aromatic character of borepin. Then, we estimated HOMA values using the optimized structures of the borepin rings in the present tri/tetracyclic systems (HOMA^{theo} in Table 4). These values of benzo[*d*]-annulated borepins were nearly 0.5 and clearly smaller than those of **1 α -Si** and **1 β -Si** as well as the parent borepin. We also estimated HOMA values from the crystal structures (HOMA^{exp}). Those of **1 α** and **1 β** were also listed in parentheses in Table 4 for comparison. Tendency of the changes of HOMA^{exp} values of tri/tetracyclic borepins, including **1 α** and **1 β** was consistent with that of HOMA^{theo}. This clearly suggests the reliability of those data, regardless of what structures were used, i.e., theoretical or experimental. The HOMA^{exp} values of benzo[*d*]-annulated borepins were nearly 0.5, again indicating their nonaromaticity. The HOMA values of the fused thiphene and benzene rings in the tri/tetracyclic systems were highly aromatic and are close to those of the parent rings (Table S2), consistent with the expectation based on the Clar structures (Figure 3C). On the basis of the NICS and HOMA estimations, it is concluded that the tetracyclic borepins is nearly “nonaromatic”. Taking the short endocyclic B–C bond lengths in the borepin ring and the observed high chemical stability of the compounds into account, the borepin ring in the present system is likely to have aromaticity to a certain extent, although the aromaticity of the tetracyclic borepins is less than that of **1 α -Si/1 α** and **1 β -Si/1 β** based on the NICS and HOMA values as mentioned above.

Electrochemical Properties. We carried out cyclic voltammetry measurements (CVs) to evaluate the redox properties of the tetracyclic borepins in DMF containing tetrabutylammonium perchlorate (0.1 M) under nitrogen. All borepins showed pseudo- or irreversible reductive waves in cathodic CVs, and their onset potentials (E_{red}) ranged from –2.03 to –2.26 V vs Fc/Fc⁺ (Figure 9, Table 2). The E_{red} values of the α -bridged borepins were higher than those of the β -bridged borepins, indicating their greater electron-accepting properties. This contrasted with the relationship between **1 α** and **1 β** , where the half-wave reduction potentials $E_{1/2 \text{ red}}$ (vs Ag/Ag⁺) of **1 α** and **1 β** were –2.42 and –2.26 V, respectively,¹⁷ but was consistent with the order of the calculated energy levels (*vide supra*). The E_{red} values shifted to lower potentials in the

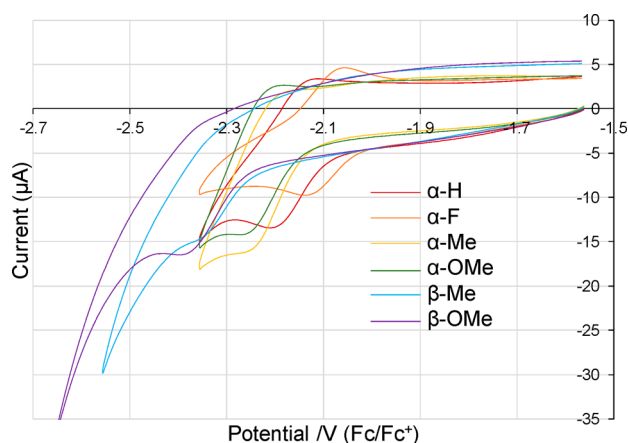


Figure 9. Cathodic CVs of benzo[*d*]-annulated borepins in DMF with 0.1 M tetrabutylammonium perchlorate as supporting electrolyte at a scan rate of 100 mV s^{−1}.

order of α -F > α -H > α -Me > α -OMe > β -Me > β -OMe, reflecting the electron-donating or electron-withdrawing properties of the substituents. Anodic CVs were also investigated. As shown in Figure S75, irreversible oxidative waves were detected for most samples, but not for α -F. The oxidative onset potentials E_{ox} were lowered with the introduction of electron-donating methoxy groups, again implying efficient control of the electronic state by the nature of the substituents.

Emission Properties in the Crystal State. Finally, we investigated the emissive properties of tetracyclic borepins in the solid state. The recrystallized samples were barely emissive ($\Phi < 2\%$), similar to the situation in solution, except for α -H ($\Phi = 18\%$) and β -OMe ($\Phi = 6\%$), and the emission color was blue except for α -H (Figures 10 and 11). To our surprise, the

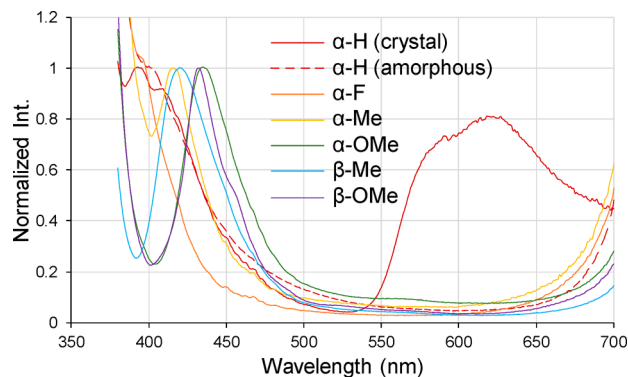


Figure 10. Fluorescence spectra of borepins in this study as solids. (excitation: 370 nm).

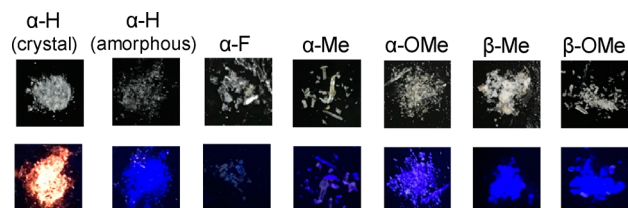


Figure 11. Photographs of borepins in this study under ambient (top) and UV (bottom) light.

emission spectrum of α -H in the crystal state contained broad bands in the 550–700 nm region, giving a reddish emission. To our knowledge, such a phenomenon has not been previously observed for borepin derivatives. To elucidate the reason for this unusual red emission, we prepared an amorphous sample of α -H by heating it in air on a hot plate at 200 °C, followed by quickly cooling the melted sample to room temperature. The amorphous form was confirmed by powder XRD analysis (Figure S76). As shown in Figure 10, the red emission at approximately 600 nm was absent in the spectrum of the amorphous sample of α -H. This indicated that crystal packing of α -H is required for the red emission. As described above, α -H has no π - π intermolecular interactions in the crystal structure (Figure 2). Therefore, this red emission is not likely to be due to excimer formation. Despite our attempts, we have not yet obtained sufficient experimental data to discuss this phenomenon in detail. Further investigations to determine the reason for this unexpected red emission are in progress and will be reported elsewhere.

CONCLUSIONS

Herein, we have reported the synthesis and properties of new benzo[*d*]dithieno[*b,f*]borepins. Benzo[*d*]annulation slightly increased deviations from planarity in the systems because of the high aromaticity of the benzene ring. As a consequence, the aromaticity of the borepin ring in the present systems was relatively lower than that of **1 α** and **1 β** , based on the results of our experimental and theoretical measurements. Despite the low aromaticity of the borepin ring, these compounds were quite stable under ambient conditions, both in solution and in solid form, especially the α -bridged borepins. Furthermore, the electrochemistry of the whole structure was influenced by substituents on the fused benzene ring, as indicated by optical and electrochemical measurements. This influence suggested that the introduction of functional groups on the benzene ring is an effective way to control the electronic structures of benzo[*d*]dithieno[*b,f*]borepin systems. Moreover, the β -bridged β -Me and β -OMe compounds showed π -stacking in the crystal structures, derived from the π -extension. This result indicated that benzo[*d*]annulation can affect not only the electronic structure but also the packing form in the crystal structure. Finally, we reported the first example of the chromic red emission of a borepin derivative, as observed for α -H in the crystal state. On the basis of the high chemical stability, tunable electronic states, and interesting emissive properties, benzo[*d*]dithieno[*b,f*]borepins are highly promising as a new class of building blocks for functional materials.

EXPERIMENTAL SECTION

General. All reactions were carried out under dry argon. Toluene, THF, and diethyl ether were purchased from Kanto Chemical Co., Ltd. and were distilled from calcium hydride and stored over activated molecular sieves under argon until use, whereas chloroform was distilled from calcium hydride immediately before use. All other chemicals were purchased from Wako Pure Chemical Industries, Ltd. and TCI Co., Ltd. Starting materials 2-tributylstannylthiophene,²⁶ 3-tributylstannylthiophene,²⁷ 1,2-dibromo-4,5-dimethylbenzene,²⁸ **1-H**,²⁹ **2-OMe**,³⁰ and **3'-OMe**³⁰ were prepared according to the literature. Mesityldimethoxyborane (MesB(OMe)₂) was prepared by a method similar to the synthesis of dimethoxytripylborane, using mesityl bromide instead of triptyl bromide.³¹ Abbreviations Bz, Th, and Mes were used for the following NMR assignments stand for fused benzene and thiophene ring, and mesityl group, respectively. NMR spectra were recorded on Varian System 500 and 400MR

spectrometers. BF₃·Et₂O and CF₃COOH were used as the external standards for ¹¹B and ¹⁹F NMR measurements, respectively. High-resolution mass spectra were obtained on a Thermo Fisher Scientific LTQ Orbitrap XL spectrometer at N-BARD, Hiroshima University.

X-ray Diffraction Analysis. Single crystal X-ray diffraction data of α -F and α -OMe were collected at 123 K on a Bruker AXS SMART APEX II ULTRA diffractometer at Natural Science Center for Basic Research and Development (N-BARD), Hiroshima University, using Mo K α radiation monochromated with a multilayered confocal mirror. The structures were solved by Intrinsic Phasing on the SHELXT-2014/4 program and expanded using Fourier techniques. Non-hydrogen atoms were refined anisotropically, whereas hydrogen atoms were included but not refined (SHELXL-2014/6). All other calculations were performed using the APEXII crystallographic software package of Bruker AXS. The data of α -H, α -Me, and β -Me, in contrast, were collected at 123 K on a Rigaku R-AXIS RAPID diffractometer using graphite-monochromated Mo K α radiation. The structures were solved by Direct Method (SIR92) and expanded using Fourier techniques. Non-hydrogen atoms were refined anisotropically, whereas hydrogen atoms were refined using the riding model by the full-matrix least-squares method. Graphical crystal structures were generated using Mercury 3.9 (Cambridge Crystallographic Data Centre). All other calculations were performed using the CRYSTAL-STRUCTURE crystallographic software package of the Rigaku Corporation. Powder XRD patterns were obtained on a Rigaku Ultima IV multipurpose X-ray diffraction system.

Photophysical Measurements. UV–vis absorption spectra were measured with a Shimadzu UV-3600 plus spectrometer. Photoluminescence (PL) spectra were measured with a HORIBA FluoroMax-4 spectrophotometer. The absolute PL quantum yields were determined by using a HORIBA FluoroMax-4 spectrophotometer attached to an integration sphere. Fluorescence decay measurements were performed on a HORIBA DeltaFlex modular fluorescence lifetime system, using a Nano LED pulsed diode excitation source.

Electrochemical Measurements. CVs were measured with a HOKUTO DENKO electrochemical measurement system HZ-7000 in a solution of 0.1 M tetrabutylammonium perchlorate (TBAP) in DMF at analyte concentrations of 2.0 mM using a three-electrode system with a Pt plate counter electrode, a Pt wire working electrode, and an Ag/Ag⁺ reference electrode.

Computational Methods. DFT calculations were performed on a Gaussian 09 program at B3LYP/6-31G(d) level of theory.³² NICS (nucleus-independent chemical shift) calculations were carried out using GIAO method at B3LYP/6-31+G(d,p) level of theory. To estimate HOMA values, we employed HOMHED indexes for C–C and C–S bonds,^{25b} whereas an experimental HOMA index was used for C–B bond.^{25a}

1,2-Bis(3-thienyl)-4,5-difluorobenzene (1-F). A mixture of 17.9 g (47.9 mmol) of 3-tributylstannylthiophene, 4.34 g (16.0 mmol) of 1,2-dibromo-4,5-difluorobenzene, 559 mg (0.484 mmol) of Pd(PPh₃)₄, and 40 mL of toluene was heated to reflux for 2 days. The mixture was cooled to room temperature and poured into a KF aqueous solution with stirring. After 3 h, the resulting suspension was filtered with Celite and washed with toluene. The organic phase was separated and washed twice with water and then once with brine. After drying the organic phase over anhydrous magnesium sulfate, the solvent was evaporated and the residue was purified by silica gel chromatography with hexane as the eluent to give 4.33 g (15.5 mmol, 97% yield) of **1-F** as a white solid. ¹H NMR (400 MHz, CDCl₃) δ : 7.24 (2H, t, *J*_{H-F} = 9.6 Hz, Bz), 7.19 (2H, dd, *J* = 3.0 and 5.1 Hz, Th), 7.04 (2H, dd, *J* = 1.3 and 3.0 Hz, Th), 6.74 (2H, dd, *J* = 1.3 and 5.1 Hz, Th). ¹³C NMR (126 MHz, CDCl₃) δ : 149.2 (dd, *J*_{C-F} = 15 and 251 Hz), 140.0, 132.0 (t, *J*_{C-F} = 5 Hz), 128.5, 125.2, 123.4, 118.7 (q, *J*_{C-F} = 6 Hz). HRMS (APCI) Calcd for C₁₄H₈F₂S₂. M⁺: 278.00300. Found: 278.00299.

4,5-Bis(3-thienyl)-o-xylene (1-Me). **1-Me** was prepared from 18.4 g (49.3 mmol) of 3-tributylstannylthiophene, 4.24 g (16.1 mmol) of 1,2-dibromo-4,5-dimethylbenzene, 557 mg (0.482 mmol) of Pd(PPh₃)₄, and 40 mL of toluene as a white solid (2.66 g, 9.84 mmol, 61% yield) in a manner similar to that above. ¹H NMR (400

MHz, CDCl₃) δ : 7.24 (s, 2H, Bz), 7.16 (2H, dd, J = 3.0 and 4.9 Hz, Th), 7.03 (2H, dd, J = 1.3 and 3.0 Hz, Th), 6.78 (2H, dd, J = 1.3 and 4.9 Hz, Th), 2.32 (6H, s, CH₃). ¹³C NMR (126 MHz, CDCl₃) δ : 142.0, 135.9, 132.8, 131.4, 129.0, 124.5, 122.4, 19.4. HRMS (APCI) Calcd for C₁₆H₁₅S₂: [M + H]⁺: 271.06097. Found: 271.06137.

4,5-Bis(2-thienyl)-o-xylene (1'-Me). 1'-Me was prepared from 18.5 g (49.6 mmol) of 2-tributylstannylthiophene and 6.27 g (23.8 mmol) of 1,2-dibromo-4,5-dimethylbenzene, 825 mg (0.714 mmol) of Pd(PPh₃)₄ and 60 mL of toluene as a colorless oil (3.99 g, 14.8 mmol, 62% yield) in a manner similar to that above. ¹H NMR (400 MHz, CDCl₃) δ : 7.29 (2H, s, Bz), 7.24 (2H, dd, J = 0.9 and 4.0 Hz, Th), 6.94 (2H, dd, J = 2.8 and 4.0 Hz, Th), 6.85 (2H, dd, J = 0.9 and 2.8 Hz, Th), 2.31 (6H, s, CH₃). ¹³C NMR (126 MHz, CDCl₃) δ : 142.7, 136.4, 132.2, 131.1, 126.8, 126.7, 125.4, 19.3. HRMS (APCI) Calcd for C₁₆H₁₅S₂: [M + H]⁺: 271.06097. Found: 271.06158.

1,2-Bis(2-bromo-3-thienyl)benzene (2-H). To a solution of 3.18 g (13.2 mmol) of 1-H in 260 mL of CHCl₃ was added 4.70 g (26.4 mmol) of NBS in several portions at 0 °C, and the reaction mixture was stirred overnight at room temperature. The reaction mixture was washed twice with water and then once with brine. After drying the organic phase over anhydrous magnesium sulfate, the solvent was evaporated to give the crude product, which was then purified by silica gel chromatography with hexane as the eluent to give 4.11 g (10.3 mmol, 78% yield) of 2-H as a light yellow solid. ¹H NMR (400 MHz, CDCl₃) δ : 7.47 (4H, m, Bz), 7.09 (2H, d, J = 5.6 Hz, Th), 6.55 (2H, d, J = 5.6 Hz, Th). ¹³C NMR (126 MHz, CDCl₃) δ : 140.9, 134.7, 130.7, 129.6, 127.9, 125.0, 110.7. HRMS (APCI) Calcd for C₁₄H₈Br₂S₂: M⁺: 397.84287. Found: 397.84280.

1,2-Bis(2-bromo-3-thienyl)-4,5-difluorobenzene (2-F). 2-F was prepared from 831 mg (2.99 mmol) of 1-F, 1.19 g (6.66 mmol) of NBS, and 30 mL of CHCl₃ in a manner similar to that above. The crude product was purified by silica gel chromatography with hexane as the eluent to give 2-F as a white viscous oil (845 mg, 1.94 mmol, 65% yield). ¹H NMR (400 MHz, CDCl₃) δ : 7.29 (2H, t, J_{H-F} = 9.5 Hz, Bz), 7.10 (2H, d, J = 5.7 Hz, Th), 6.51 (2H, d, J = 5.7 Hz, Th). ¹³C NMR (126 MHz, CDCl₃) δ : 149.5 (dd, J_{C-F} = 15 and 252 Hz), 138.9, 131.5 (t, J_{C-F} = 5 Hz), 129.2, 125.5, 119.6 (q, J_{C-F} = 6 Hz), 111.4. HRMS (APCI) Calcd for C₁₄H₆Br₂F₂S₂: M⁺: 433.82402. Found: 433.82404.

4,5-Bis(2-bromo-3-thienyl)-o-xylene (2-Me). 2-Me was prepared from 813 mg (3.01 mmol) of 1-Me, 1.06 g (6.00 mmol) of NBS, and 30 mL of CHCl₃ in a manner similar to that above. The crude product was purified by silica gel chromatography with dichloromethane as the eluent to give 2-Me as a light yellow solid (1.16 g, 2.71 mmol, 90% yield). ¹H NMR (400 MHz, CDCl₃) δ : 7.25 (2H, s, Bz), 7.08 (2H, d, J = 5.6 Hz, Th), 6.54 (2H, d, J = 5.6 Hz, Th), 2.35 (6H, s, CH₃). ¹³C NMR (126 MHz, CDCl₃) δ : 140.9, 136.5, 132.0, 131.8, 129.8, 124.8, 110.4, 19.6. HRMS (APCI) Calcd for C₁₆H₁₂Br₂S₂: M⁺: 425.87417. Found: 425.87448.

4,5-Bis(3,5-dibromo-2-thienyl)-o-xylene (2'-Me). 2'-Me was prepared from 1.09 g (4.02 mmol) of 1'-Me, 2.93 g (16.5 mmol) of NBS, 40 mL of CHCl₃, and 40 mL of acetic acid in a manner similar to that above. The crude product was purified by preparative GPC with toluene as the eluent to give 2'-Me as a colorless viscous oil (879 mg, 1.50 mmol, 37% yield). ¹H NMR (400 MHz, CDCl₃) δ : 7.26 (2H, s, Bz), 6.92 (2H, s, Th), 2.34 (6H, s, CH₃). ¹³C NMR (126 MHz, CDCl₃) δ : 138.3, 138.0, 132.9, 132.3, 129.3, 112.7, 109.7, 19.6. HRMS (APCI) Calcd for C₁₆H₁₀Br₄S₂: M⁺: 581.69519. Found: 581.69531.

1,2-Bis(2-bromo-5-trimethylsilyl-3-thienyl)benzene (3-H). To a solution of 1.79 g (4.47 mmol) of 2-H in 45 mL of ether was added 8.1 mL (9.2 mmol) of 1.13 M LDA in THF/hexane at -78 °C over a period of 5 min and the mixture was stirred at this temperature for 10 min then at 0 °C for 50 min. To this was added 1.23 mL (9.74 mmol) of trimethylsilyl chloride at -78 °C, and the mixture was stirred at room temperature overnight. The resulting mixture was hydrolyzed with water. The organic layer was separated and the aqueous layer was extracted with 100 mL of ethyl acetate. The combined organic layers were washed twice with water and once with brine. After drying over anhydrous magnesium sulfate, the solvent was evaporated, and the residue was purified by silica gel chromatography

with hexane as the eluent to give 1.74 g (3.20 mmol, 72% yield) of 3-H as a colorless viscous oil. ¹H NMR (400 MHz, CDCl₃) δ : 7.51–7.42 (4H, m, Bz), 6.58 (2H, s, Th), 0.19 (18H, s, Si-CH₃). ¹³C NMR (126 MHz, CDCl₃) δ : 142.1, 140.3, 136.4, 134.8, 130.4, 127.7, 115.2, -0.3. HRMS (APCI) Calcd for C₂₀H₂₅Br₂S₂Si₂: [M + H]⁺: 542.92975. Found: 542.93011.

4,5-Bis(2-bromo-5-trimethylsilyl-3-thienyl)-o-xylene (3-Me). 3-Me was prepared from 1.16 g (2.71 mmol) of 2-Me, 4.90 mL (5.54 mmol) of 1.13 M LDA in THF/hexane, 0.86 mL (6.81 mmol) of trimethylsilyl chloride, and 30 mL of ether as a white solid (1.03 g, 1.79 mmol, 66% yield) in a manner similar to that above. ¹H NMR (400 MHz, CDCl₃) δ : 7.26 (2H, s, Bz), 6.57 (2H, s, Th), 2.34 (6H, s, C-CH₃), 0.19 (18H, Si-CH₃). ¹³C NMR (126 MHz, CDCl₃) δ : 142.1, 140.0, 136.6, 136.2, 132.1, 131.4, 114.9, 19.6, -0.3. HRMS (APCI) Calcd for C₂₂H₂₈Br₂S₂Si₂: M⁺: 569.95322. Found: 569.95313.

4,5-Bis(3-bromo-5-trimethylsilyl-2-thienyl)-o-xylene (3'-Me). To a solution of 565 mg (0.965 mmol) of 2'-Me in 15 mL of ether was added 1.20 mL (1.97 mmol) of 1.64 M *n*BuLi in hexane at -78 °C over a period of 5 min, and the mixture was stirred at this temperature for 20 min. To this was added 0.31 mL (2.45 mmol) of trimethylsilyl chloride at this temperature and the mixture was stirred at room temperature overnight. The resulting mixture was hydrolyzed with water. The organic layer was separated, and the aqueous layer was extracted with 50 mL of ethyl acetate. The combined organic layers were washed twice with water and then once with brine. After drying over anhydrous magnesium sulfate, the solvent was evaporated, and the residue was purified by silica gel chromatography with hexane as the eluent to give 328 mg (0.572 mmol, 59% yield) of 3'-Me as a white solid. ¹H NMR (400 MHz, CDCl₃) δ : 7.31 (2H, s, Bz), 6.99 (2H, s, Th), 2.34 (6H, s, C-CH₃), 0.24 (18H, s, Si-CH₃). ¹³C NMR (126 MHz, CDCl₃) δ : 142.0, 141.1, 137.1, 136.1, 132.4, 130.4, 111.5, 19.6, -0.4. HRMS (APCI) Calcd for C₂₂H₂₈Br₂S₂Si₂: M⁺: 569.95322. Found: 569.95319.

Compound α -H. To a solution of 265 mg (0.486 mmol) of 3-H in 5 mL of ether was added 0.61 mL (1.0 mmol) of 1.64 mol/L *n*BuLi in hexane at -78 °C over a period of 5 min, and the mixture was stirred at this temperature for 20 min. To this was added 145 mg (0.755 mmol) of MesB(OMe)₂ at this temperature, and the mixture was stirred at room temperature overnight. The resulting mixture was hydrolyzed with water, and 30 mL of ethyl acetate was added. The organic layer was separated, and the aqueous layer was extracted with 30 mL of ethyl acetate. The combined organic layers were washed twice with water and then once with brine. After drying over anhydrous magnesium sulfate, the solvent was evaporated. The crude product was purified by preparative GPC with toluene as the eluent to give 163 mg (0.316 mmol, 65% yield) of α -H as a white solid. This solid was recrystallized by slow evaporation from hexane for XRD analysis and emission measurements in the solid state. ¹H NMR (400 MHz, CDCl₃) δ : 8.38–8.34 (2H, m, Bz), 8.17 (2H, s, Th), 7.59–7.54 (2H, m, Bz), 6.94 (2H, s, Mes), 2.40 (3H, s, *p*-CH₃, Mes), 2.11 (6H, s, *o*-CH₃, Mes), 0.36 (18H, s, Si-CH₃). ¹³C NMR (126 MHz, CDCl₃) δ : 151.6, 151.3, 149.1 (br, B-C), 141.4 (br, B-C), 138.6, 137.8 (Th ring CH), 137.2, 133.2, 131.4 (Bz ring CH), 127.2 (Bz ring CH), 127.1 (Mes ring CH), 23.0 (*o*-CH₃, Mes), 21.5 (*p*-CH₃, Mes), -0.1 (Si-CH₃). ¹¹B NMR (160 MHz, CDCl₃) δ : 51.1 ($w_{1/2}$ = 1900 Hz). HRMS (APCI) Calcd for C₂₉H₃₅BS₂Si₂: M⁺: 514.18063. Found: 514.18103.

Compound α -F-H. Compound α -F-H was prepared from 369 mg (0.847 mmol) of 2-F, 1.05 mL (1.72 mmol) of 1.64 M *n*BuLi in hexane, 203 mg (1.06 mmol) of MesB(OMe)₂, and 5 mL of ether in a manner similar to that above. The crude product was purified by silica gel chromatography with a mixed solvent of hexane/dichloromethane = 2/1 as the eluent to give α -F-H as a white solid (199 mg, 0.498 mmol, 58% yield). This solid was recrystallized by slow evaporation from acetonitrile containing a small amount of dichloromethane to give single crystals for XRD analysis and emission measurements in the solid state. ¹H NMR (400 MHz, CDCl₃) δ : 8.14 (2H, t, J_{H-F} = 10.7 Hz, Bz), 7.99 (2H, d, J = 5.1 Hz, Th), 7.96 (2H, d, J = 5.1 Hz, Th), 6.92 (2H, s, Mes), 2.39 (3H, s, *p*-CH₃, Mes), 2.08 (6H, s, *o*-CH₃, Mes). ¹³C NMR (126 MHz, CDCl₃) δ : 148.8 (dd, J_{C-F} = 15 and 252

H_z), 148.8, 144.6 (br, B–C), 140.5 (br, B–C), 138.7, 137.7, 135.9 (Th ring CH), 131.1 (Th ring CH), 130.5 (t, $J_{C-F} = 4$ Hz), 127.2 (Mes ring CH), 119.6 (q, $J_{C-F} = 6$ Hz, Bz ring CH), 22.8 (*o*-CH₃, Mes), 21.4 (*p*-CH₃, Mes). ¹¹B NMR (160 MHz, CDCl₃) δ : 50.9 ($w_{1/2} = 900$ Hz). ¹⁹F NMR (470 MHz, CDCl₃) δ : -138.3 (m). HRMS (APCI) Calcd for C₂₃H₁₇BF₂S₂: M⁺: 406.08273. Found: 406.08289.

Compound α -Me. Compound α -Me was prepared from 238 mg (0.416 mmol) of **3-Me**, 0.52 mL (0.85 mmol) of 1.64 M *n*BuLi in hexane, 104 mg (0.541 mmol) of MesB(OMe)₂, and 5 mL of ether in a manner similar to that above. The crude product was purified by preparative GPC with toluene as the eluent to give α -Me as a white solid (115 mg, 0.212 mmol, 51% yield). This solid was recrystallized by slow evaporation from acetonitrile containing a small amount of dichloromethane to give single crystals for XRD analysis and emission measurements in the solid state. ¹H NMR (400 MHz, CDCl₃) δ : 8.15 (2H, s, Th), 8.10 (2H, s, Bz), 6.92 (2H, s, Mes), 2.48 (6H, s, CH₃, Bz), 2.39 (3H, s, *p*-CH₃, Mes), 2.10 (6H, s, *o*-CH₃, Mes), 0.36 (18H, s, Si-CH₃). NOESY NMR was taken to assign the two signals at 8.15 and 8.10 ppm in the ¹H NMR spectrum (Figure S39). ¹³C NMR (126 MHz, CDCl₃) δ : 151.4, 151.3, 148.6 (br, B–C), 141.6 (br, B–C), 138.6, 137.6 (Th ring CH), 137.1, 136.0, 132.2 (Bz ring CH), 131.1, 127.1 (Mes ring CH), 22.9 (*o*-CH₃, Mes), 21.5 (*p*-CH₃, Mes), 19.8 (CH₃, Bz), -0.1 (Si-CH₃). ¹¹B NMR (160 MHz, CDCl₃) δ : 50.3 ($w_{1/2} = 1900$ Hz). HRMS (APCI) Calcd for C₃₁H₃₉BS₂Si₂: M⁺: 542.21193. Found: 542.21210.

Compound α -OMe-H. Compound α -OMe-H was prepared from 230 mg (0.501 mmol) of **2-OMe**, 0.63 mL (1.0 mmol) of 1.64 M *n*BuLi in hexane, 123 mg (0.640 mmol) of MesB(OMe)₂, and 10 mL of a 1:1 mixed solvent of ether and THF in a manner similar to that above. The crude product was purified by silica gel chromatography with a mixed solvent of hexane/dichloromethane = 1/1 as the eluent to give α -OMe-H as a white solid (91.9 mg, 0.214 mmol, 43% yield). ¹H NMR (400 MHz, CDCl₃) δ : 8.08 (2H, d, $J = 5.1$ Hz, Th), 7.94 (2H, d, $J = 5.1$ Hz, Th), 7.80 (2H, s, Bz), 6.93 (2H, s, Mes), 4.09 (6H, s, OCH₃), 2.39 (3H, s, *p*-CH₃, Mes), 2.09 (6H, *o*-CH₃, Mes). ¹³C NMR (126 MHz, CDCl₃) δ : 150.5, 148.3, 138.8, 137.4, 135.3 (Th ring CH), 130.8 (Th ring CH), 127.5, 127.1 (Mes ring CH), 113.2 (Bz ring CH), 55.9 (OCH₃), 22.8 (*o*-CH₃, Mes), 21.4 (*p*-CH₃, Mes). Two signals for B–C were not detected, probably due to their low intensities. ¹¹B NMR (160 MHz, CDCl₃) δ : 49.7 ($w_{1/2} = 1100$ Hz). HRMS (APCI) Calcd for C₂₅H₂₃BO₂S₂: M⁺: 430.12270. Found: 430.12262.

Compound β -Me. Compound β -Me was prepared from 141 mg (0.247 mmol) of **3'-Me**, 0.45 mL (0.74 mmol) of 1.64 M *n*BuLi in hexane, 85.7 mg (0.446 mmol) of MesB(OMe)₂, and 5 mL of ether in a manner similar to that above. The crude product was purified by preparative GPC with toluene as the eluent, followed by silica gel chromatography with a mixed solvent of hexane/dichloromethane = 1/1 as the eluent to give β -Me as a white solid (60.7 mg, 0.112 mmol, 45% yield). This solid was recrystallized by slow evaporation from acetonitrile containing a small amount of dichloromethane to give single crystals for XRD analysis and emission measurements in the solid state. ¹H NMR (400 MHz, CDCl₃) δ : 8.22 (2H, s, Bz), 7.34 (2H, s, Th), 6.89 (2H, s, Mes), 2.44 (6H, s, CH₃, Bz), 2.39 (3H, s, *p*-CH₃, Mes), 1.98 (6H, *o*-CH₃, Mes), 0.30 (18H, s, Si-CH₃). ¹³C NMR (126 MHz, CDCl₃) δ : 162.0, 146.0 (br, B–C), 144.5 (Th ring CH), 138.1, 137.32, 137.25, 135.9, 132.5 (Bz ring CH), 128.6, 126.9 (Mes ring CH), 22.7 (*o*-CH₃, Mes), 21.3 (*p*-CH₃, Mes), 19.7 (CH₃, Bz), 0.0 (Si-CH₃). One signal for B–C was not detected, probably due to the low intensity. ¹¹B NMR (160 MHz, CDCl₃) δ : 55.1 ($w_{1/2} = 1600$ Hz). HRMS (APCI) Calcd for C₃₁H₃₉BS₂Si₂: M⁺: 542.21193. Found: 542.21222.

Compound β -OMe. Compound β -OMe was prepared from 334 mg (0.553 mmol) of **3'-OMe**, 0.70 mL (1.1 mmol) of 1.64 M *n*BuLi in hexane, 145 mg (0.755 mmol) of MesB(OMe)₂, and 5 mL of ether in a manner similar to that above. The crude product was purified by preparative GPC with toluene as the eluent, followed by silica gel chromatography with a mixed solvent of hexane/dichloromethane = 1/1 as the eluent to give β -OMe as a white solid (110 mg, 0.192 mmol, 35% yield). This solid was recrystallized from dichloromethane

by vapor diffusion with acetonitrile as the precipitant to give single crystals for XRD analysis and emission measurements in the solid state. ¹H NMR (400 MHz, CDCl₃) δ : 7.85 (2H, s, Bz), 7.35 (2H, s, Th), 6.90 (2H, s, Mes), 4.10 (6H, s, OCH₃), 2.39 (3H, s, *p*-CH₃, Mes), 1.98 (6H, s, *o*-CH₃, Mes), 0.31 (18H, s, Si-CH₃). ¹³C NMR (126 MHz, CDCl₃) δ : 161.8, 149.0, 145.7 (br, B–C), 144.9 (Th ring CH), 144.0 (br, B–C), 137.9, 137.4, 135.9, 126.9 (Mes ring CH), 125.0, 112.9 (Bz ring CH), 56.0 (OCH₃), 22.7 (*o*-CH₃, Mes), 21.3 (*p*-CH₃, Mes), -0.1 (Si-CH₃). ¹¹B NMR (160 MHz, CDCl₃) δ : 54.4 ($w_{1/2} = 1700$ Hz). HRMS (APCI) Calcd for C₃₁H₃₉BO₂S₂Si₂: M⁺: 574.20176. Found: 574.20239.

Compound α -F. To a solution of 57.2 mg (0.141 mmol) of α -F-H in 5 mL of ether was added 0.19 mL (0.31 mmol) of 1.61 M *t*BuLi in pentane at -78 °C over a period of 5 min and the mixture was stirred at this temperature for 30 min. To this was added 0.055 mL (0.44 mmol) of trimethylsilyl chloride at this temperature, and the mixture was stirred at room temperature overnight. The resulting mixture was hydrolyzed with water, and 30 mL of ethyl acetate was added. The organic layer was separated, and the aqueous layer was extracted with 50 mL of ethyl acetate. The combined organic layers were washed twice with water and then once with brine. After drying over anhydrous magnesium sulfate, the solvent was evaporated, and the residue was purified by preparative GPC with toluene as the eluent to give 40.6 mg (0.0737 mmol, 52% yield) of α -F as a white solid. This solid was recrystallized by slow evaporation from acetonitrile to give single crystals for XRD analysis and emission measurements in the solid state. ¹H NMR (400 MHz, CDCl₃) δ : 8.13 (2H, t, $J_{H-F} = 10.7$ Hz, Bz), 8.02 (2H, s, Th), 6.94 (2H, s, Mes), 2.40 (3H, s, *p*-CH₃, Mes), 2.09 (6H, s, *o*-CH₃, Mes), 0.36 (18H, s, Si-CH₃). ¹³C NMR (126 MHz, CDCl₃) δ : 152.6, 149.3, 148.7 (dd, $J_{C-F} = 15$ and 252 Hz), 138.6, 137.5 (Th ring CH), 137.4, 130.5 (t, $J_{C-F} = 4$ Hz), 127.2 (Mes ring CH), 119.5 (q, $J_{C-F} = 6$ Hz, Bz ring CH), 22.9 (*o*-CH₃, Mes), 21.5 (*p*-CH₃, Mes), -0.2 (Si-CH₃). Two signals for B–C were not detected. ¹¹B NMR (160 MHz, CDCl₃) δ : 50.8 ($w_{1/2} = 1300$ Hz). ¹⁹F NMR (470 MHz, CDCl₃) δ : -138.9 (m). HRMS (APCI) Calcd for C₂₉H₃₃BF₂S₂Si₂: M⁺: 550.16178. Found: 550.16180.

Compound α -OMe. To a solution of 67.2 mg (0.156 mmol) of α -OMe-H in 10 mL of a 1:1 mixed solvent of ether and THF was added 0.35 mL (0.40 mmol) of 1.13 M LDA in THF/hexane at -78 °C over a period of 5 min, and the mixture was stirred at 0 °C for 30 min. To this was added 0.060 mL (0.47 mmol) of trimethylsilyl chloride at this temperature, and the mixture was stirred at room temperature overnight. The resulting mixture was hydrolyzed with water, and 30 mL of ethyl acetate was added. The organic layer was separated, and the aqueous layer was extracted with 50 mL of ethyl acetate. The combined organic layers were washed twice with water and then once with brine. After drying over anhydrous magnesium sulfate, the solvent was evaporated, and the residue was purified by preparative GPC with toluene as the eluent to give 25.5 mg (0.044 mmol, 28% yield) of α -OMe as a white solid. ¹H NMR (400 MHz, CDCl₃) δ : 8.09 (2H, s, Th), 7.78 (2H, s, Bz), 6.94 (2H, s, Mes), 4.09 (6H, s, OCH₃), 2.40 (3H, s, *p*-CH₃, Mes), 2.11 (6H, *o*-CH₃, Mes), 0.36 (18H, s, Si-CH₃). ¹³C NMR (126 MHz, CDCl₃) δ : 151.7, 151.0, 148.1, 138.7, 137.24 (Th ring CH), 137.15, 127.5, 127.1 (Mes ring CH), 113.4 (Bz ring CH), 56.0 (OCH₃), 22.9 (*o*-CH₃, Mes), 21.5 (*p*-CH₃, Mes), -0.1 (Si-CH₃). ¹¹B NMR (160 MHz, CDCl₃) δ : 50.5 ($w_{1/2} = 1500$ Hz). HRMS (APCI) Calcd for C₃₁H₃₉BO₂S₂Si₂: M⁺: 574.20176. Found: 574.20233.

■ ASSOCIATED CONTENT

● Supporting Information

The Supporting Information is available free of charge on the ACS Publications website at DOI: 10.1021/acs.organomet.7b00844.

Experimental details, NMR spectra, fluorescence spectra, anodic CVs, and theoretical calculations (PDF)

X-ray crystallographic data (XYZ)

Accession Codes

CCDC 1587388–1587392 contain the supplementary crystallographic data for this paper. These data can be obtained free of charge via www.ccdc.cam.ac.uk/data_request/cif, or by emailing data_request@ccdc.cam.ac.uk, or by contacting The Cambridge Crystallographic Data Centre, 12 Union Road, Cambridge CB2 1EZ, UK; fax: +44 1223 336033.

AUTHOR INFORMATION

Corresponding Author

*Tel.: +81-82-424-7743. Fax: +81-82-424-5494. E-mail: jo@hiroshima-u.ac.jp

ORCID

Joji Ohshita: 0000-0002-5401-514X

Notes

The authors declare no competing financial interest.

ACKNOWLEDGMENTS

This work was supported by JSPS KAKENHI Grant NOS. JP17H06890 AND JP17H03105. We thank Prof. Kazuyoshi Tanaka (Kyoto University) for his kind support on NICS calculations.

REFERENCES

- (1) (a) Schulman, J. M.; Disch, R. L.; Sabio, M. L. *J. Am. Chem. Soc.* **1982**, *104*, 3785–3788. (b) Disch, R. L.; Sabio, M. L.; Schulman, J. M. *Tetrahedron Lett.* **1983**, *24*, 1863–1866. (c) Subramanian, G.; Schleyer, P. von R.; Jiao, H. *Organometallics* **1997**, *16*, 2362–2369. (d) Schulman, J. M.; Disch, R. L. *Organometallics* **2000**, *19*, 2932–2936.
- (2) Leusink, A. J.; Drenth, W.; Noltes, J. G.; van der Kerk, G. J. M. *Tetrahedron Lett.* **1967**, *8*, 1263–1266.
- (3) (a) van Tamelen, E. E.; Brieger, G.; Untch, K. G. *Tetrahedron Lett.* **1960**, *1*, 14–15. (b) Axelrad, G.; Halpern, D. *J. Chem. Soc. D* **1971**, *0*, 291.
- (4) (a) Eisch, J. J.; Galle, J. E. *J. Am. Chem. Soc.* **1975**, *97*, 4436–4437. (b) Eisch, J. J.; Galle, J. E.; Shafii, B.; Rheingold, A. L. *Organometallics* **1990**, *9*, 2342–2349.
- (5) Gronowitz, S.; Gassne, P.; Yom-Tov, B.; Heinegård, D.; Balaban, A. T.; Craig, J. C. *Acta Chem. Scand.* **1969**, *23*, 2927–2930.
- (6) (a) Sugihara, Y.; Miyatake, R.; Yagi, T. *Chem. Lett.* **1993**, *22*, 933–936. (b) Sugihara, Y.; Yagi, T.; Murata, I.; Imamura, A. *J. Am. Chem. Soc.* **1992**, *114*, 1479–1481. (c) Sugihara, Y.; Miyatake, R.; Yagi, T.; Murata, I.; Jinguji, M.; Nakazawa, T.; Imamura, A. *Tetrahedron* **1994**, *50*, 6495–6504.
- (7) Sugihara, Y.; Miyatake, R.; Murata, I.; Imamura, A. *J. Chem. Soc., Chem. Commun.* **1995**, *0*, 1249–1250.
- (8) (a) Miyata, M.; Chujo, Y. *Polym. J.* **2002**, *34*, 967–969. (b) Matsumi, N.; Chujo, Y. *Polym. J.* **2008**, *40*, 77–89. (c) Nagai, A.; Murakami, T.; Nagata, Y.; Kokado, K.; Chujo, Y. *Macromolecules* **2009**, *42*, 7217–7220.
- (9) (a) Li, H.; Jäkle, F. *Angew. Chem., Int. Ed.* **2009**, *48*, 2313–2316. (b) Li, H.; Jäkle, F. *Macromol. Rapid Commun.* **2010**, *31*, 915–920. (c) Chen, P.; Jäkle, F. *J. Am. Chem. Soc.* **2011**, *133*, 20142–20145. (d) Chen, P.; Lalancette, R. A.; Jäkle, F. *Angew. Chem., Int. Ed.* **2012**, *51*, 7994–7998. (e) Chen, P.; Yin, X.; Baser-Kirazli, N.; Jäkle, F. *Angew. Chem., Int. Ed.* **2015**, *54*, 10768–10772.
- (10) (a) Yin, X.; Chen, J.; Lalancette, R. A.; Marder, T. B.; Jäkle, F. *Angew. Chem., Int. Ed.* **2014**, *53*, 9761–9765. (b) Yin, X.; Guo, F.; Lalancette, R. A.; Jäkle, F. *Macromolecules* **2016**, *49*, 537–546. (c) Yin, X.; Liu, K.; Ren, Y.; Lalancette, R. A.; Loo, Y.-L.; Jäkle, F. *Chem. Sci.* **2017**, *8*, 5497–5505.
- (11) (a) Yamaguchi, S.; Tamao, K. *Chem. Lett.* **2005**, *34*, 2–7. (b) Yamaguchi, S.; Tamao, K. *J. Chem. Soc., Dalton Trans.* **1998**, *0*, 3693–3702. (c) Hissler, M.; Dyer, P. W.; Réau, R. *Coord. Chem. Rev.* **2003**, *244*, 1–44. (d) Baumgartner, T.; Réau, R. *Chem. Rev.* **2006**, *106*, 4681–4727.
- (12) (a) Shuto, A.; Kushida, T.; Fukushima, T.; Kaji, H.; Yamaguchi, S. *Org. Lett.* **2013**, *15*, 6234–6237. (b) Kushida, T.; Shuto, A.; Yoshio, M.; Kato, T.; Yamaguchi, S. *Angew. Chem., Int. Ed.* **2015**, *54*, 6922–6925. (c) Yamaguchi, S.; Wakamiya, A. *Pure Appl. Chem.* **2006**, *78*, 1413–1424. (d) Jäkle, F. *Chem. Rev.* **2010**, *110*, 3985–4022. (e) Ren, Y.; Jäkle, F. *Dalton Trans.* **2016**, *45*, 13996–14007.
- (13) (a) Murata, H.; Malliaras, G. G.; Uchida, M.; Shen, Y.; Kafafi, Z. H. *Chem. Phys. Lett.* **2001**, *339*, 161–169. (b) Murata, H.; Kafafi, Z. H.; Uchida, M. *Appl. Phys. Lett.* **2002**, *80*, 189–191.
- (14) Parke, S. M.; Boone, M. P.; Rivard, E. *Chem. Commun.* **2016**, *52*, 9485–9505.
- (15) Mercier, L. G.; Piers, W. E.; Parvez, M. *Angew. Chem., Int. Ed.* **2009**, *48*, 6108–6111.
- (16) Caruso, A., Jr.; Siegler, M. A.; Tovar, J. D. *Angew. Chem., Int. Ed.* **2010**, *49*, 4213–4217.
- (17) Levine, D. R.; Siegler, M. A.; Tovar, J. D. *J. Am. Chem. Soc.* **2014**, *136*, 7132–7139.
- (18) (a) Caruso, A., Jr.; Tovar, J. D. *J. Org. Chem.* **2011**, *76*, 2227–2239. (b) Caruso, A., Jr.; Tovar, J. D. *Org. Lett.* **2011**, *13*, 3106–3109. (c) Levine, D. R.; Caruso, A., Jr.; Siegler, M. A.; Tovar, J. D. *Chem. Commun.* **2012**, *48*, 6256–6258. (d) Messersmith, R. E.; Siegler, M. A.; Tovar, J. D. *J. Org. Chem.* **2016**, *81*, 5595–5605. (e) Levine, D. R.; Messersmith, R. E.; Siegler, M. A.; Tovar, J. D. *Can. J. Chem.* **2017**, *95*, 381–389. (f) Messersmith, R. E.; Yadav, S.; Siegler, M. A.; Ottosson, H.; Tovar, J. D. *J. Org. Chem.* **2017**, *82*, 13440–13448.
- (19) Iida, A.; Saito, S.; Sasamori, T.; Yamaguchi, S. *Angew. Chem., Int. Ed.* **2013**, *52*, 3760–3764.
- (20) Schickedanz, K.; Radtke, J.; Bolte, M.; Lerner, H.-W.; Wagner, M. *J. Am. Chem. Soc.* **2017**, *139*, 2842–2851.
- (21) Lee, H.; Cha, I.; Lee, E. J.; Lee, Y.; Kim, Y. H.; Song, C. *Chem. Lett.* **2014**, *43*, 1432–1434.
- (22) Ren, Y.; Sezen, M.; Guo, F.; Jäkle, F.; Loo, Y.-L. *Chem. Sci.* **2016**, *7*, 4211–4219.
- (23) Solà, M. *Front. Chem.* **2013**, *1*, 22.
- (24) Ghosh, D.; Periyasamy, G.; Pati, S. K. *Phys. Chem. Chem. Phys.* **2011**, *13*, 20627–20636.
- (25) (a) Zborowski, K. K.; Alkorta, I.; Elguero, J.; Proniewicz, L. M. *Struct. Chem.* **2012**, *23*, 595–600. (b) Frizzo, C. P.; Martins, M. A. P. *Struct. Chem.* **2012**, *23*, 375–380. (c) Green, J. P.; Cryer, S. J.; Marafie, J.; White, A. J. P.; Heeney, M. *Organometallics* **2017**, *36*, 2632–2636.
- (26) Istanbuluoğlu, C.; Göker, S.; Hizalan, G.; Hacıoğlu, S. O.; Udum, Y. A.; Yildiz, E. D.; Cirpan, A.; Toppare, L. *New J. Chem.* **2015**, *39*, 6623–6630.
- (27) Leliège, A.; Régent, C.-H. L.; Allain, M.; Blanchard, P.; Roncali, J. *Chem. Commun.* **2012**, *48*, 8907–8909.
- (28) Chen, Z.; Dong, S.; Zhong, C.; Zhang, Z.; Niu, L.; Li, Z.; Zhang, F. *J. Photochem. Photobiol., A* **2009**, *206*, 213–219.
- (29) Yoshida, H.; Okada, K.; Kawashima, S.; Tanino, K.; Ohshita, J. *Chem. Commun.* **2010**, *46*, 1763–1765.
- (30) Weis, J. G.; Swager, T. M. *ACS Macro Lett.* **2015**, *4*, 138–142.
- (31) Wan, W.-M.; Cheng, F.; Jäkle, F. *Angew. Chem., Int. Ed.* **2014**, *53*, 8934–8938.
- (32) Frisch, M. J.; Trucks, G. W.; Schlegel, H. B.; Scuseria, G. E.; Robb, M. A.; Cheeseman, J. R.; Scalmani, G.; Barone, V.; Mennucci, B.; Petersson, G. A.; Nakatsuji, H.; Caricato, M.; Li, X.; Hratchian, H. P.; Izmaylov, A. F.; Bloino, J.; Zheng, G.; Sonnenberg, J. L.; Hada, M.; Ehara, M.; Toyota, K.; Fukuda, R.; Hasegawa, J.; Ishida, M.; Nakajima, T.; Honda, Y.; Kitao, O.; Nakai, H.; Vreven, T.; Montgomery, J. A., Jr.; Peralta, J. E.; Ogliaro, F.; Bearpark, M.; Heyd, J. J.; Brothers, E.; Kudin, K. N.; Staroverov, V. N.; Kobayashi, R.; Normand, J.; Raghavachari, K.; Rendell, A.; Burant, J. C.; Iyengar, S. S.; Tomasi, J.; Cossi, M.; Rega, N.; Millam, J. M.; Klene, M.; Knox, J. E.; Cross, J. B.; Bakken, V.; Adamo, C.; Jaramillo, J.; Gomperts, R.; Stratmann, R. E.; Yazyev, O.; Austin, A. J.; Cammi, R.; Pomelli, C.; Ochterski, J. W.; Martin, R. L.; Morokuma, K.; Zakrzewski, V. G.; Voth, G. A.; Salvador, P.; Dannenberg, J. J.; Dapprich, S.; Daniels, A. D.; Farkas, O.;

Foresman, J. B.; Ortiz, J. V.; Cioslowski, J.; Fox, D. J. *Gaussian 09*, revision A.02; Gaussian, Inc.: Wallingford, CT, 2009.